Duplex Stainless Steel Fracture Surface Analysis Using X-ray Fractography

K. Rajanna, B. Pathiraj, and B.H. Kolster

The fatigue fracture surface of a duplex stainless steel was analyzed using x-ray fractography. A lower than average austenite content was observed at the fracture surface due to the transformation of austenite into deformation-induced martensite. The influence of fatigue cycling on the transformation was confined to a depth of about 30 μm below the fracture surface. X-ray analyses of both the ferrite-martensite and the austenite phases indicated residual stresses (σ_r) increasing with depth from the fracture surface and reaching a maximum some tens of microns below the fracture surface. The lower σ_r observed at the fracture surface has been attributed to the stress relaxation effects caused by the new fracture surfaces created in the crack growth process. The observed decrease in full width at half maximum (FWHM) in the ferrite-martensite phase was presumed to be due to the dynamic recovery effect that was likely to occur within the material close to the crack tip as a consequence of fatigue cycling.

Keywords

duplex stainless steel, dynamic recovery, full width at half maximum, residual stress, stress relaxation, X-ray fractography

1. Introduction

X-RAY fractography is a technique in which a fracture surface is examined using x-ray diffraction (XRD) methods (Ref 1). Variations in the residual stress (σ_r) and the full width at half maximum (FWHM, denoted by B) of the diffraction profile are determined as a function of the maximum stress-intensity factor (K_{max}) and the depth (y) below the fracture surface. So far this technique has been employed to examine the fracture surface of materials such as high-strength aluminum alloys (Ref 2), structural steels (Ref 3-5), austenitic stainless steel (Ref 6, 7), and ceramics (Ref 8). This investigation examines a duplex stainless steel using this method.

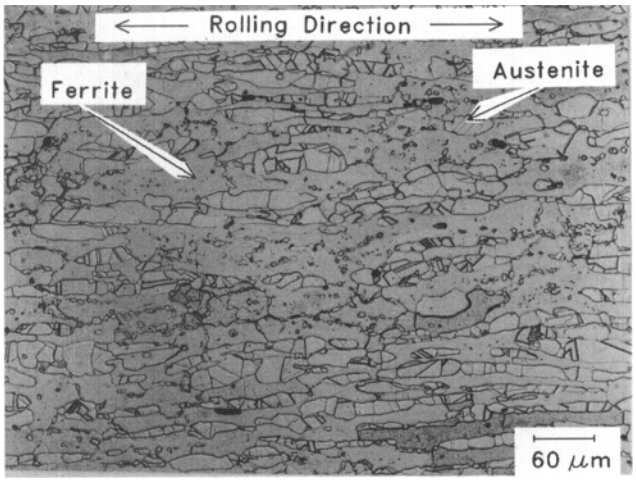

Fig. 1 Typical microstructure of the duplex stainless steel. Electrolytically etched with 10% oxalic acid

Duplex steels are known for their corrosion resistance coupled with excellent tensile, fatigue, and impact strengths (even at low temperatures) (Ref 9). In general, their chemical compositions and thermal treatments are adjusted such that the steel contains nearly equal parts of ferrite and austenite. This near-equal proportion results in optimum strength, formability, and weldability (Ref 10).

A duplex steel with about 50% ferrite and 50% austenite was selected for this investigation. The variations in σ_r and B as a function of K_{max} and depth below the surface were examined for both the ferrite-martensite and the austenite phases of the steel. Attempts were made to correlate the x-ray results with features revealed by scanning electron microscopy (SEM) and transmission electron microscopy (TEM).

2. Experimental Details

The material investigated was A790-grade duplex stainless steel and was obtained in the form of 10 mm thick hot-rolled bar. The steel was solution annealed between 1050 and 1100 °C and water quenched. The chemical composition of this steel, as provided by the supplier, was Fe-0.024C-1.60Mn-0.33Si-0.021P-0.001S-5.5Ni-19.6Cr-2.85Mo (in weight percent).

A small sample was cut from the bar and examined for microstructural analysis along the rolling direction. The sample was prepared by mechanical means, and later electrolytically etched in 10% oxalic acid using a current density of 1 A/cm^2 for 1 min. The etched surface was then examined under an optical microscope. A representative microstructure of the original steel before fatigue testing consisted of elongated austenite grains in the ferrite matrix (Fig. 1). The average grain sizes of the two phases when measured in the width direction were found to be about 30 μm.

Compact tension specimens, 12.5 mm thick, were prepared from the rolled bar for use in fatigue crack growth tests. Figure

K. Rajanna, Foundation for Advanced Metals Science (SGM), Hengelo, The Netherlands (presently at Metallurgy Department, Corporate R&D Division, B.H.E.L., Vikas Nagar, Hyderabad-500 593, India); **B. Pathiraj** and **B.H. Kolster,** Foundation for Advanced Metals Science (SGM), Hengelo, The Netherlands (presently at Department of Mechanical Engineering, University of Twente, 7500 AE Enschede, The Netherlands).

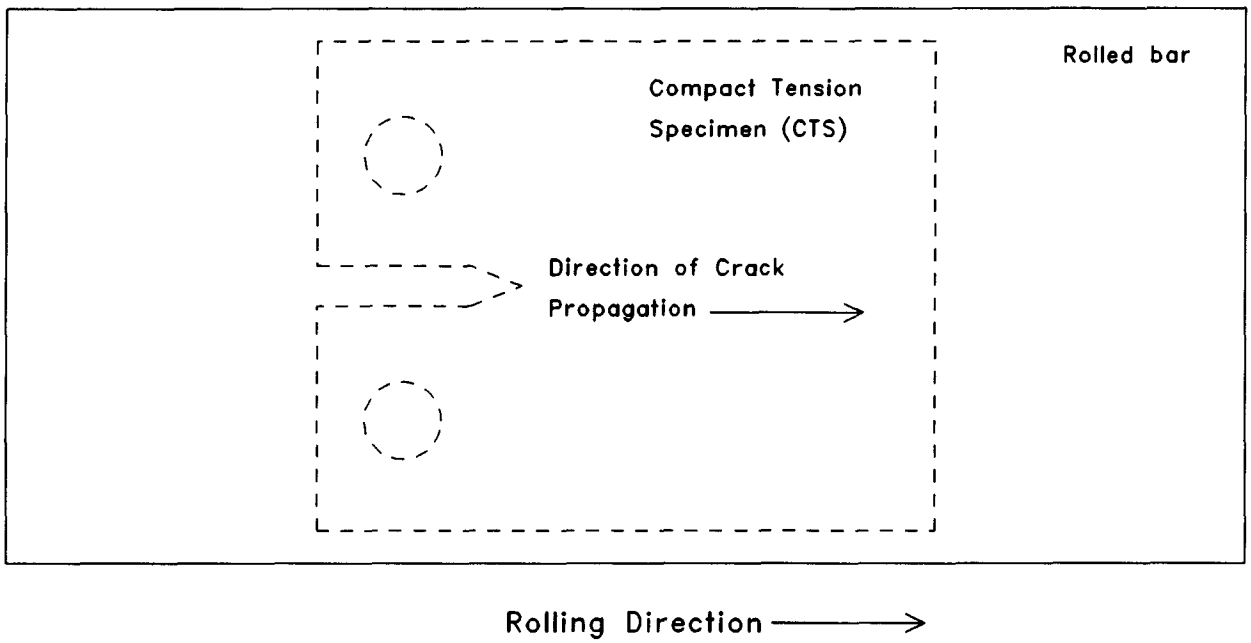

Fig. 2 Orientation of the test specimen with reference to rolling direction of the bar

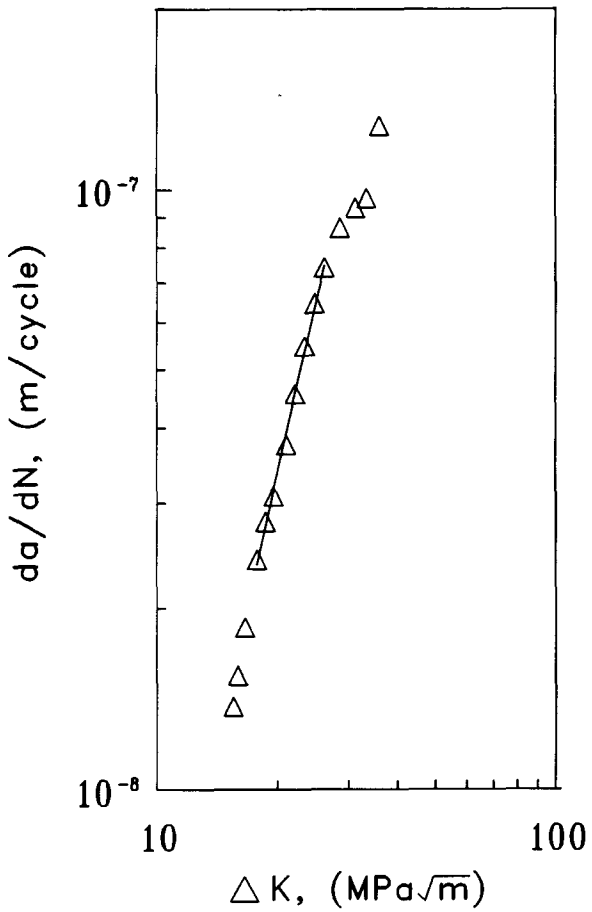

Fig. 3 Log (*da/dN*) versus log ΔK plot obtained for the duplex stainless steel

2 shows the orientation of the test specimen with reference to the rolling direction. This notch configuration was chosen so that the fatigue crack would propagate in the rolling direction. Fatigue tests were carried out according to the ASTM E 647 standard procedure. All tests were performed in a ±100 kN static-dynamic servohydraulic test system, using a stress ratio (R) of 0.1 and a frequency of 20 Hz.

One of the fracture surfaces was examined by high-resolution SEM to analyze the fracture morphologies at different crack length positions corresponding to different K_{max} levels. X-ray residual stress measurements were subsequently performed at these locations using the standard multiple-exposure $\sin^2\psi$ method (Ref 11). A portable x-ray stress analyzer using filtered Cr-Kα radiation was employed for this purpose. The ferrite and austenite contents of the steel were determined by comparing the integrated intensities of the XRD profiles of the (211) ferrite and the (220) austenite reflections. The stress measurements were performed on both the ferrite and the austenite phases using the respective reflections. The residual stress measurement system was automated for carrying out measurements continuously at preselected locations. This was achieved by means of software developed for moving the specimen to the next preselected location for measurement soon after completing the measurement at a particular location. The x-ray-irradiated area was restricted to a strip approximately 10 mm long and 1 mm wide. This was achieved by attaching an additional slit with a suitable opening to the soller slit assembly of the x-ray goniometer at the source side. Subsurface x-ray analysis was performed by successive layer removal of the material by electropolishing. The thickness of material removed was measured by a precision-type dial gage to an accuracy of ±1 μm.

A few 2 mm disk-type TEM samples were prepared at different locations from the second half portion of the test specimen. Such samples were prepared from material lying below the fracture surface at a depth of about 30 μm. These were examined in a 200 kV high-resolution TEM.

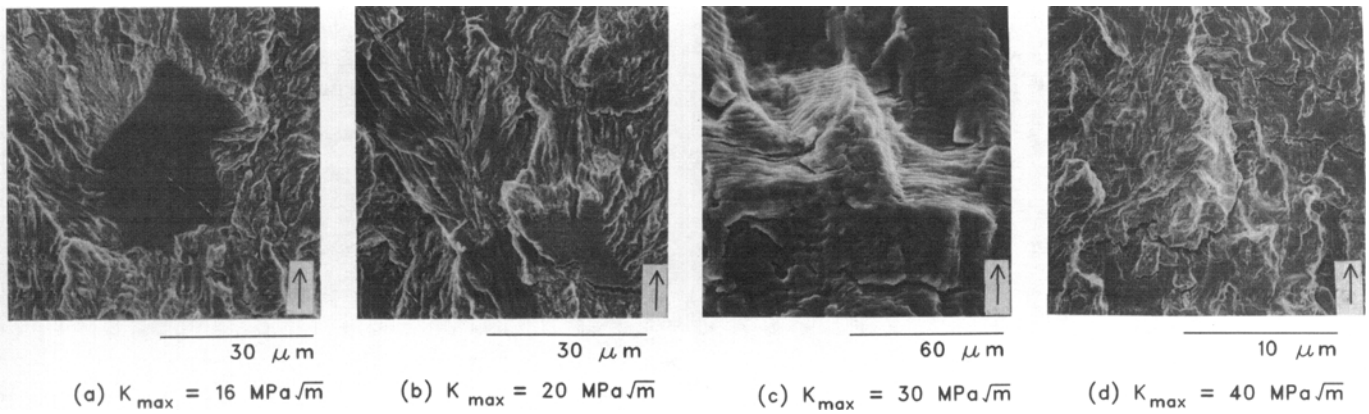

Fig. 4 Representative SEM fractographs at different K_{max} levels in the duplex stainless steel. Arrows indicate the direction of crack propagation.

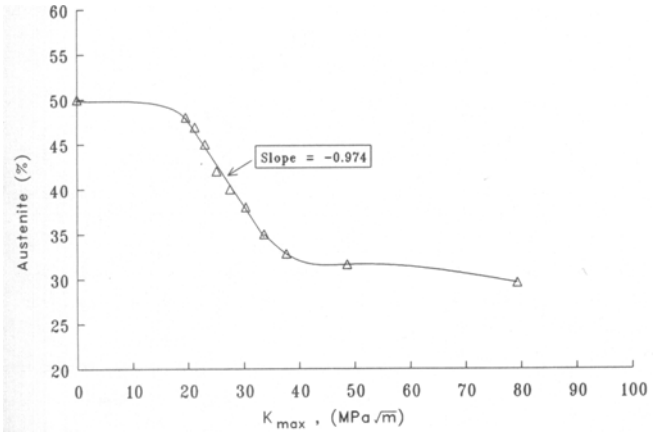

Fig. 5 Variation in austenite content with K_{max}

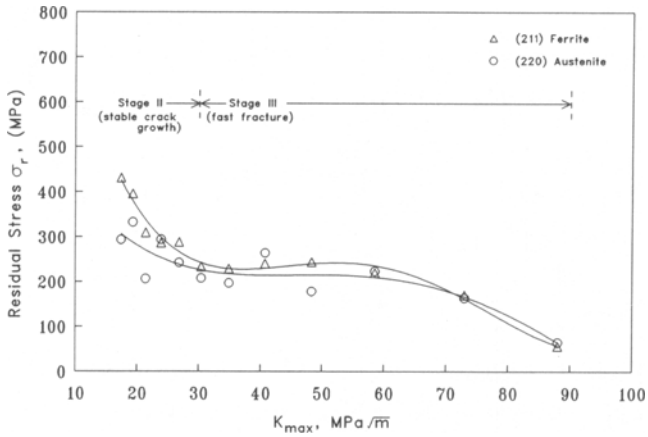

Fig. 6 Residual stress, σ_r, distribution as a function of K_{max}

3. Results and Discussion

3.1 *Fatigue Crack Growth Tests*

The log (*da/dN*) versus log ΔK plot is shown in Fig. 3. The stable crack growth is limited up to a ΔK value of about 30 MPa$\sqrt{m}$. The slope of the plot (m) is 3.06, somewhat smaller than the value of about 3.30 obtained with fully austenitic stainless steels (Ref 7). The absolute *da/dN* values at any K_{max} were also found to be far smaller than those obtained for austenitic stainless steels (Ref 7) and C45-grade ferritic steel (Ref 5).

3.2 *SEM Analysis of the Fracture Surface*

Representative fracture morphologies are shown in Fig. 4(a) to (d) as a function of K_{max}. Figures 4(a) and (b) show quasi-cleavage features observed in the K_{max} range of 16 to 30 MPa$\sqrt{m}$ (stage II region). Some localized dark shaded regions with typical fatigue striations are visible in Fig. 4(a) and (b). As K_{max} approaches 30 MPa$\sqrt{m}$, the fracture morphologies indicate typical fatigue striations (Fig. 4c). This K_{max} value approximately coincides with that at which the fast fracture region begins. At the fast fracture locations where K_{max} is greater than 40 MPa$\sqrt{m}$, the fracture consisted of quasi-cleavage features (Fig. 4d).

3.3 *X-ray Analysis of the Fracture Surface*

The variation in the austenite content was examined at different locations of the fracture surface and is shown in Fig. 5 as a function of K_{max}. A maximum decrease of about 20% in austenite content from the base composition (50%) is apparent. The variation in the austenite content is approximately linear up to about 35 MPa$\sqrt{m}$. No further significant decrease is observed at K_{max} values greater than 40 MPa$\sqrt{m}$. The decrease in austenite content is considered to be a consequence of the formation of deformation-induced martensite as a result of plastic strain at the crack tip. The differences noticed in the variation of the austenite content as a function of K_{max} (Fig. 5) may perhaps be related to the differences in the fatigue behavior of the individual phases of the duplex steel due to the plastic strain cycling. Magnin et al. (Ref 12) investigated the low-cycle fatigue (LCF) behavior of similar duplex stainless steel by studying the deformation mechanisms of individual phases of the steel. It was shown that at low strain amplitudes ($\Delta\varepsilon_p/2 < 10^{-3}$), the LCF behavior of the steel was controlled by the cyclic deformation of the austenite. On the other hand, at high strain amplitudes ($\Delta\varepsilon_p/2 > 10^{-3}$), the cyclic deformation behavior of the ferrite was found to control the LCF properties of the duplex steel. In the latter case, it was also noticed that even if the austenite was plastically deformed, crack initiation in ferrite

(α) occurs early so that the fatigue resistance of the austenite (γ) phase does not influence the behavior of the duplex alloy. Following these observations, the present result could be explained by assuming that the plastic strains are small within 35 $MPa\sqrt{m}$ and are accommodated in the austenite phase, resulting in its transformation to strain-induced martensite.

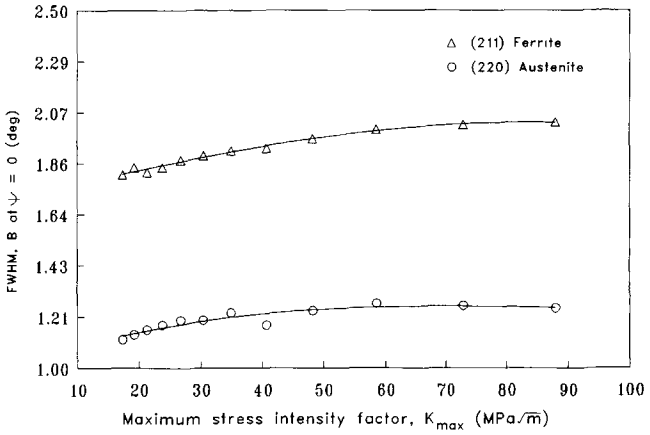

Fig. 7 FWHM (B) distribution as a function of K_{max}

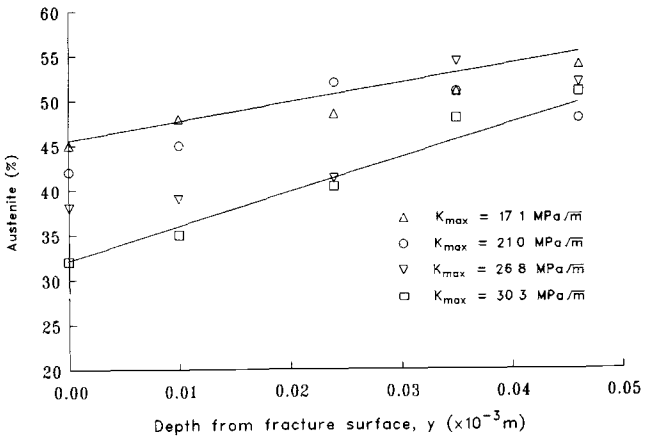

Fig. 8 Variation in austenite content with depth below the fracture surface

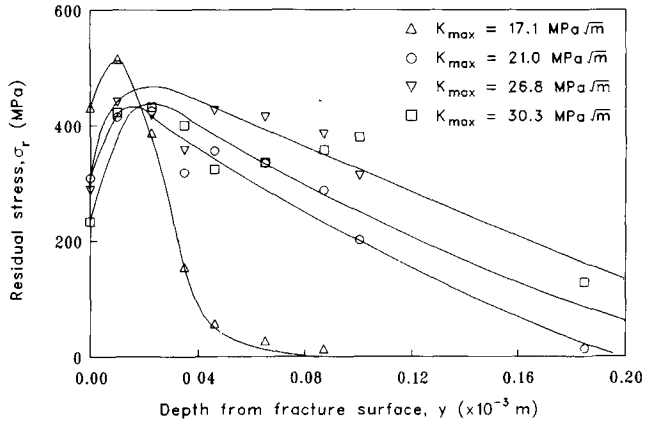

(a)

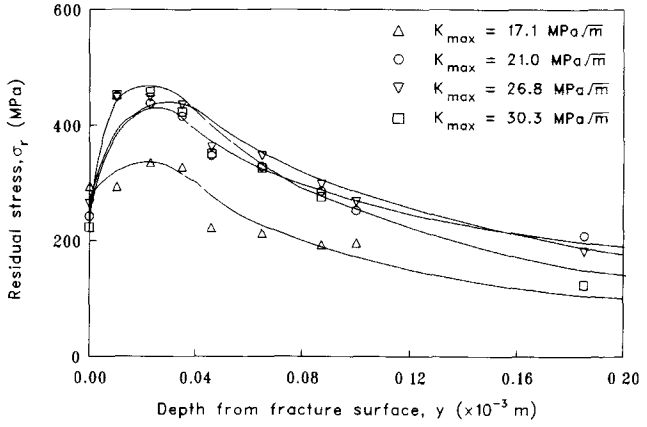

(b)

Fig. 9 Residual stress, σ_r, distribution as a function of depth below the fracture surface. (a) Ferrite-martensite phase. (b) Austenite phase

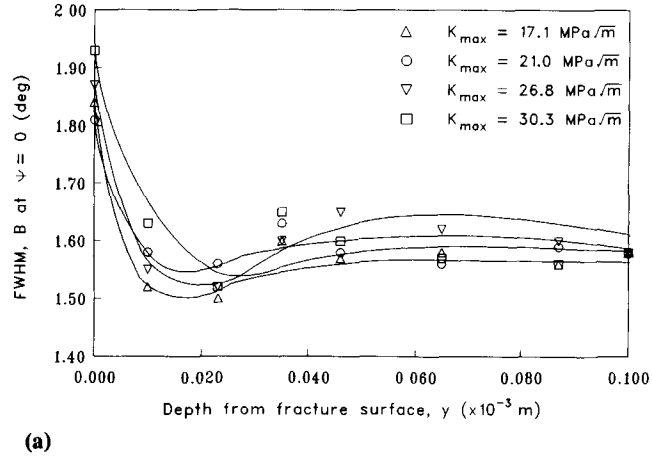

(a)

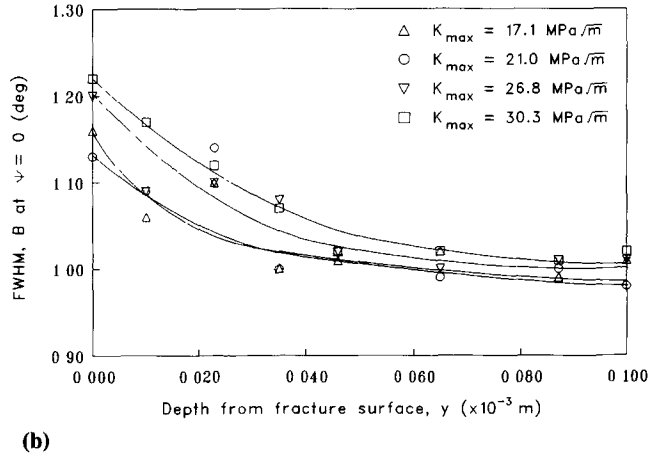

(b)

Fig. 10 FWHM (B) distribution as a function of depth below the fracture surface. (a) Ferrite-martensite phase. (b) Austenite phase

The σ_r variations with K_{max} are shown in Fig. 6 for both the ferrite-martensite and the austenite phases. At all locations the stresses are tensile. No significant differences in the σ_r distributions of either phases are noticed except at very low K_{max} levels. The corresponding B variations with K_{max} are shown in Fig. 7 for both phases. The overall B-K_{max} variations in both phases appear to be marginal, and the B values for the ferrite-martensite are always larger than those for the austenite.

3.4 *Subsurface X-ray Analysis*

The variation in austenite content for different K_{max} values was determined as a function of depth (y) below the fracture surface. The results obtained are shown in Fig. 8. The austenite content was found to approach the base material composition of 50% at a depth of about 30 μm.

The σ_r variations as a function of depth below the fracture surface for the ferrite-martensite and the austenite phases are shown in Fig. 9(a) and (b), respectively. In both cases, the σ_r was found to increase to a maximum within a depth of a few tens of microns below the fracture surface. Thereafter, a gradual decrease to a minimum was noticed at greater depths. The lower σ_r value observed at the fracture surface is due to the relaxation of the elastic component of the total stress-strain developed within the plastically deformed region ahead of the crack tip. The creation of free surfaces due to the crack growth process could result in such a stress relaxation.

The corresponding B variations with depth for the ferrite-martensite and the austenite phases of the steel are shown in Fig. 10(a) and (b), respectively. They show a gradual decrease to about 1.56° for the ferrite-martensite phase and to about 1.00° for the austenite phase. The variations in the ferrite-martensite phase (Fig. 10a) within a depth of a few tens of microns below the fracture surface show trends with a decrease in B followed by a small increase. This resulted in a minimum value of B within these depths. These depths were presumed to refer to the extent of the material damage as a consequence of fatigue cycling wherein some dynamic recovery in ferrite could have occurred. Similar observations have been made in the analysis of C45 steel specimens tested in different heat-treated conditions (Ref 7). The dynamic recovery aspect was examined by analyzing several samples, prepared from material close to these depths, in a 200 kV high-resolution TEM. The representative micrographs, shown in Fig. 11 for the ferrite-martensite phase, indicate the variations in the dislocation density and their arrangement as a function of K_{max}. They also indicate the presence of some dynamic recovery (Fig. 11b) in at least a few locations. The B-y variations for the austenite phase did not show a minimum B value below the fracture surface, indicating no recovery effects.

4. Conclusions

- The da/dN value at any K_{max} was found to be lower in a duplex stainless steel than in fully austenitic steels.
- The fracture morphologies indicated quasi-cleavage features within the stable crack growth region. Some localized areas were found to contain fatigue striations.
- A linear increase in martensite content and K_{max} was noticed up to about 35 MPa$\sqrt{m}$. A maximum increase of about 20% in the martensite content was noticed within this range of K_{max}. This was considered to be a consequence of the

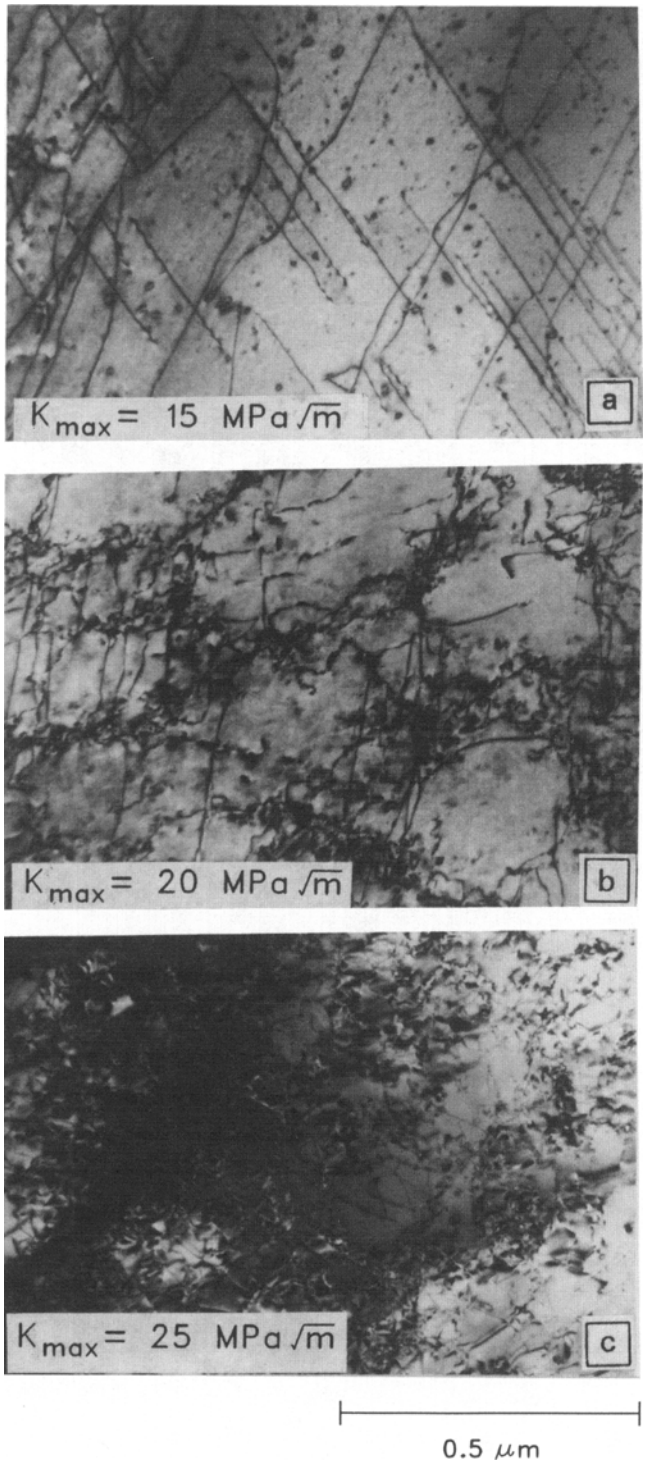

Fig. 11 Representative TEM micrographs for the observations made at 30 μm below the fracture surface at different K_{max} levels in the ferrite phase of the duplex stainless steel

formation of deformation-induced martensite due to the plastic strain cycling effects ahead of the crack tip.

- Both the ferrite (α) and austenite (γ) phases were found to contain tensile residual stresses (σ_r) at the fracture surface, and no significant differences were noticed in the σ_r variation with K_{max}.
- The overall variation of the diffraction profile breadth (B) with K_{max} was observed to be marginal in both phases. The B value for the ferrite-martensite was larger than that for the austenite at any K_{max}.
- The amount of deformation-induced martensite was found to decrease with depth below the fracture surface and to approach the base composition (50%) at a depth of about 30 μm.
- The σ_r distributions with depth exhibited maxima at a depth of a few tens of microns below the fracture surface for both the ferrite-martensite and the austenite phases. The minimum σ_r at the fracture surface has been attributed to the possible relaxation of the elastic stress due to the new fracture surfaces created by the growing crack.
- The B variations with depth exhibited minima within a few microns of depth below the fracture surface in the ferrite-martensite phase, indicating a possible dynamic recovery. This was confirmed by some TEM investigations performed on samples taken from depths just close to the fracture surface. In austenite, no such trends were noticed.

Acknowledgment

The authors gratefully acknowledge the technical assistance of Ir. P. Danker and Ir. M.A. Smithers of the Foundation for Advanced Metals Science (SGM), The Netherlands.

References

1. Committee on X-ray Study on Mechanical Behaviour of Materials, X-ray Fractography, *J. Soc. Mater. Sci.*, Vol 31, 1982, p 244-252
2. A. Suzuki, A. Tanji, Z. Yajima, Y. Hirose, and K. Tanaka, X-ray Diffraction Study of Fracture Surface Made by Fracture Toughness Tests of Blunt Notched CT Specimens of Aluminium Alloy, *Adv. X-ray Anal.*, Vol 30, 1986, p 537-544
3. J.L. Lebrun, M. Barral, A. Bignonnet, C. Maillard-Salin, and A. Nhari, X-ray Fractography: A New Technique for Fatigue Crack Growth and Failure Analysis, *Proc. Conf. Residual Stress in Science and Technology,* Vol 1, Garmisch-Partenkirchen, Germany, 1986, p 109-116
4. Y. Hirose, Z. Yajima, and T. Mura, X-ray Fractography on Fatigue Fracture Surfaces of AISI 4340 Steel, *Adv. X-ray Anal.*, Vol 29, 1985, p 63-70
5. K. Rajanna, B. Pathiraj, and B.H. Kolster, Fatigue Fracture Surface Analysis in C45 Steel Specimens Using X-ray Fractography, *Eng. Fract. Mech.*, Vol 39, 1991, p 147-157
6. Y. Yoshioka and B. Guimard, X-ray Fractographic Study on the Fatigue Fractured Stainless Steels, *Proc. 2nd Int. Conf. Residual Stresses (ICRS2),* G. Beck, S. Denis, and A. Simon, Ed., Elsevier Applied Science, Essex, U.K., 1989, p 852-857
7. K. Rajanna, "X-ray Fractographic Studies on Ferritic, Austenitic and Duplex Steels," University of Twente, Enschede, The Netherlands, May 1991
8. T. Mishima, Y. Nanayama, Y. Hirose, and K. Tanaka, X-ray Fractography of Fracture Surface of Alumina Ceramics, *Adv. X-ray Anal.*, Vol 30, 1986, p 545-552
9. K. Takizawa, Y. Shimizu, E. Yoneda, and I. Tamura, *Trans. Iron Steel Inst. Jpn.*, 1982, p 325-332
10. H.W. Schlapfer and J. Weber, *Mater. Tech.*, Vol 2, 1986, p 60-69
11. E. Macherauch and P. Muller, Das $Sin^2\psi$—Verfahren der rontgenographischen spannungsmessung, *Z. Angew. Phys.*, Vol 13, 1961, p 305-312
12. T. Magnin, J.M. Lardon, and L. Coudreuse, A New Approach to Low Cycle Fatigue Behaviour of a Duplex Stainless Steel Based on the Deformation Mechanisms of the Individual Phases, *Low Cycle Fatigue,* STP 942, H.D. Solomon et al., Ed., ASTM, 1988, p 812-823